Journal of Marine Science and Technology

Volume 23 | Issue 6 Article 5

COMPARISON BETWEEN CONSISTENT COUPLED-MODE SYSTEM AND EIGENFUNCTION MATCHING METHOD FOR SOLVING WATER WAVE SCATTERING

Chia-Cheng Tsai
Department of Marine Environmental Engineering, National Kaohsiung Marine University, Kaohsiung and International Wave Dynamics Research Center, National Cheng Kung University, Tainan, Taiwan, R.O.C.,
tsaichiacheng@mail.nkmu.edu.tw

Wan-Rong Chou
Department of Marine Environmental Engineering, National Kaohsiung Marine University, Kaohsiung and Department of Hydraulic and Ocean Engineering, National Cheng Kung University, Tainan, Taiwan, R.O.C.

Journal of Marine Science and Technology, Vol. 23, No. 6, pp. 870-881 (2015)
DOI: 10.6119/JMST-015-0610-4

COMPARISON BETWEEN CONSISTENT COUPLED-MODE SYSTEM AND EIGENFUNCTION MATCHING METHOD FOR SOLVING WATER WAVE SCATTERING

Chia-Cheng Tsai[1] and Wan-Rong Chou[2]

Key words: eigenfunction matching method, coupled modes, mild-slope equation, integral equation method, Roseau's analytical solution.

ABSTRACT

Both the consistent coupled-mode system (CCMS) and the eigenfunction matching method (EMM) are well-known models for simulating the propagation of small-amplitude water waves over variable bathymetry. In this study, a thorough comparison is performed through numerical experiments. For the CCMS, a bottom-sloping mode is coupled in the mild-slope equation with evanescent modes, then the CCMS are discretized by the finite-element method with high-order shape functions. For the EMM, the bottom profile is approximated in terms of successive flat shelves separated by abrupt steps, and then eigensolutions on the shelves are matched by the conservation of mass and momentum. To perform error analysis, numerical solutions are compared with Roseau's analytical solution and the semi-analytical solutions of the integral equation method. Numerical results indicate that the CCMS and EMM are accurate up to six and four decimal places, respectively. On the other hand, the EMM is more efficient for short waves because multiple waves can be approximated by few shelves. In addition, improvements in their accuracy over the mild-slope system without bottom-sloping mode are shown to be significant.

I. INTRODUCTION

The problem of water wave scattering by a bed of arbitrary topography is of considerable interest to coastal engineers, and continues to receive attention. Although the nonlinear effects become significant as the shoreline is approached, a consistent linear solution is still very useful and provides extensive information concerning the wave field and its impact on the nearshore and coastal environments. In addition, linear theory usually serves as the basis for weakly nonlinear models.

Because analytic solutions are rare except for the cases of constant bottom and Roseau's (1976) profile, numerical solutions are required for solving problems of water wave scattering. For example, Berkhoff (1972) derived the mild-slope equation (MSE) by removing the vertical coordinate using the integration of depth function, and hence reducing the dimensionality of the considered problem by one. Kirby (1986) extended the MSE by including a rapidly varying topography and applied the derived equation to the Bragg scattering of waves passing over sinusoidal beds. Chamberlain and Porter (1995) further modified the MSE by adding the bottom curvature and slope-squared terms into the traditional MSE by Berkhoff (1972). A significant restriction for any of the prescribed one-equation models is that the vertical structure of the wave field is given by a specific depth function. Therefore, these models cannot totally resolve water wave scattering over complicated bottom topography. Further improvements were made by considering the propagating and all evanescent modes and deriving a hierarchy of MSEs (Massel, 1993; Porter and Staziker, 1995), denoted as the mild-slope system (MSS) in this study. The vertical modes of the MSS have zero vertical derivative at the local depth; therefore, this model is inconsistent for problems with the Neumann condition on a sloping bottom. Athanassoulis and Belibassakis (1999) improved the model by including a sloping-bottom mode and deriving the consistent coupled-mode system (CCMS). The CCMS have been applied for a variety of water wave problems (Belibassakis et al., 2001; Belibassakis and Athanassoulis, 2002; Belibassakis, 2007; Athanassoulis and Belibassakis, 2009).

Alternatively, there are eigenfunction matching methods (EMMs), in which the bed profile under consideration is approximated by a sequence of flat shelves separated by abrupt

Paper submitted 11/06/14; revised 01/20/15; accepted 06/10/15. Author for correspondence: Chia-Cheng Tsai (e-mail:tsaichiacheng@mail.nkmu.edu.tw).
[1] Department of Marine Environmental Engineering, National Kaohsiung Marine University, Kaohsiung and International Wave Dynamics Research Center, National Cheng Kung University, Tainan, Taiwan, R.O.C.
[2] Department of Marine Environmental Engineering, National Kaohsiung Marine University, Kaohsiung and Department of Hydraulic and Ocean Engineering, National Cheng Kung University, Tainan, Taiwan, R.O.C.

steps and the solution on each shelf is constructed by eigenfunctions. The EMMs can be classified into the indirect (Newman, 1965; Miles, 1967; Mei and Black, 1969; Devillard et al., 1988; O'Hare and Davies, 1992; O'Hare and Davies, 1993; Tsai et al., 2011; Tsai et al., 2014) and direct methods (Takano, 1960; Kirby and Dalrymple, 1983; Rey, 1992; Rey, 1995; Bender and Dean, 2003; Tsai et al., 2013; Seo, 2014). Recently, Tsai et al. (2011; 2014) demonstrated that the numerical accuracy of the indirect and direct EMMs is the same, although the latter method is simpler. In addition, the resulted matrix of the direct EMM is sparse and can be solved efficiently either by sparse matrix solvers, such as the SuperLU (James et al., 1999), or the transfer matrix formulation (Seo, 2014). Therefore, we will focus only on the direct EMM and denote it as the EMM in the following of this study.

As a first impression, one may conclude that the MSE-type models are better than the EMMs, in both efficiency and accuracy, when solving problems of water wave scattering over an arbitrary smoothly varying bottom topography. However, O'Hare and Davies (1993) demonstrated that the numerical solutions of the extended MSE (Kirby, 1986) and the indirect EMM with wide-space assumption (Devillard et al., 1988; O'Hare and Davies, 1992) are comparably accurate. Recently, Tsai et al. (2014) demonstrated the superiority of the EMM over the MSS in terms of accuracy (Massel, 1993; Porter and Staziker, 1995); both require similar computational cost when they are solved by the sparse matrix solver SuperLU (James et al., 1999). These results invite us to perform a detailed comparison between the CCMS, the MSS, and the EMM. Currently, the applications of EMM are limited to stationary problems in two-dimensional or three-dimensional axisymmetric domains (Bender and Dean, 2005).

To perform error analysis for the CCMS, MSS, and EMM, numerical results are compared with Roseau's analytical solution (1976). Furthermore, we consider Porter and Porter's study (2000), in which an integral equation method (IEM) was developed to obtain highly accurate solutions for water wave scattering by a step of arbitrary profile. In that study, they declared that their semi-analytical solutions were accurate up to six decimal places by floating-point computing. In this study, we carefully reproduced their method for solving water wave scattering by sinusoidal shoal and slope, and compared the results with the numerical results of the CCMS, MSS, and EMM.

This paper is organized as follows: the wave problem is mathematically modeled in Section 2. Next, the CCMS and EMM are reviewed in Sections 3 and 4, respectively. Numerical comparisons are performed in Section 5 and the conclusions are drawn in Section 6.

II. WAVE MODEL

We consider a two-dimensional problem for a monochromatic wave propagating over an arbitrary bottom configuration with time dependence $e^{-\mathbf{i}\omega t}$, where t is the time, ω is the angular frequency, and $\mathbf{i}=\sqrt{-1}$ is the unit of complex numbers, as depicted in Fig. 1. In the figure, the coordinate (x, y) is defined such that x is the horizontal direction and y is the vertical direction positively upward from the still water level on $y = 0$. It is assumed that the bottom slope exhibits an arbitrary one-dimensional variation in a subdomain of finite length lying between two regions of constant but different depths, $h = h_-$ and $h = h_+$ for $x \le L_-$ and $x \ge L_+$, respectively.

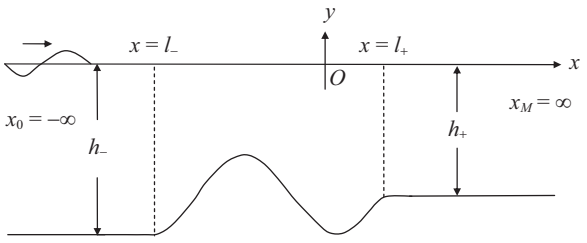

Fig. 1. Configuration of problem definition.

Furthermore, the bottom profile is described by

$$y=-h(x) \text{ for } L_- \le x \le L_+ \tag{1}$$

with $h(L_-)=h_-$ and $h(L_+)=h_+$.

According to Airy's (1845) linear wave theory, the velocity potential, $\Phi(x, y)$, is governed by the Laplace equation as

$$\nabla^2\Phi = 0, \tag{2}$$

and subject to the free surface conditions

$$\frac{\partial\Phi}{\partial y} - K\Phi = 0 \text{ on } y = 0 \tag{3}$$

and

$$-\mathbf{i}\omega\Phi + g\eta = 0 \text{ on } y = 0, \tag{4}$$

and the bottom boundary condition

$$\frac{\partial\Phi}{\partial y} + \frac{\partial\Phi}{\partial x}\frac{dh}{dx} = 0 \text{ on } y = -h(x), \tag{5}$$

where $K=\dfrac{\omega^2}{g}$, with g the acceleration of gravity. In Eq. (4), η is the surface elevation relative to the still water level.

Furthermore, the following far-field conditions are required to make the solution unique:

$$\begin{cases} \eta = e^{\mathbf{i}k_- x} + Re^{-\mathbf{i}k_- x} & as \;\; x \to -\infty \\ \eta = Te^{\mathbf{i}k_+ x} & as \;\; x \to \infty, \end{cases} \tag{6}$$

where R and T are the reflection and transmission coefficients,

respectively. In Eq. (6), we have assumed that the amplitude of the incident wave is one without loss of generality. Before introducing the solution procedure, it should be mentioned that R and T are the desired solutions to be obtained.

III. CONSISTENT COUPLED-MODE SYSTEM

Athanassoulis and Belibassakis (1999) used the variational formulation for deriving the CCMS. In this study, we alternatively utilize the Galerkin method, which has been used for deriving the MSS (Massel, 1993). First, the Galerkin method is applied to the governing Eq. (2) for obtaining

$$\int_{-h(x)}^{0} f_l\left(y,h(x)\right)\left(\frac{\partial^2\Phi}{\partial x^2}+\frac{\partial^2\Phi}{\partial y^2}\right)dy=0 \text{ for } l=-1, 0, 1, 2, \ldots , \tag{7}$$

where $f_l\left(y,h(x)\right)$ is the depth function, defined as

$$\begin{cases} f_{-1}\left(y,h(x)\right)=h(x)\left[\left(\dfrac{y}{h(x)}\right)^3+\left(\dfrac{y}{h(x)}\right)^2\right] \\ f_l\left(y,h(x)\right)=\dfrac{\cosh k_l\left(y+h(x)\right)}{\cosh k_l h(x)} \text{ for } l=0, 1, 2, \ldots , \end{cases} \tag{8}$$

where the propagating wavenumber, k_0, and evanescent wavenumbers, k_1, k_2, ..., are respectively the positive real and pure imaginary roots of the dispersion relation:

$$k_m \tanh k_m h(x)=K \tag{9}$$

To be more precise, the evanescent wavenumbers can be alternatively defined as $k_m=\mathbf{i}\kappa_m$ with $\kappa_1<\kappa_2<\kappa_3<$, ..., and

$$-\kappa_m \tan k_m h(x)=K \text{ for } l=1, 2, 3, \ldots . \tag{10}$$

In Eq. (8), the choice of the depth function for the sloping-bottom mode is not unique and has been further explained in the literature (Athanassoulis and Belibassakis, 1999).

Then, we can expand the desired solution as

$$\Phi(x,y)=\sum_{n=-1}^{\infty} f_n\left(y,h(x)\right)\phi_n(x). \tag{11}$$

Substituting Eq. (11) into Eq. (7) and performing some mathematical manipulations can result in the CCMS, as follows:

$$\sum_{n=-1}^{\infty}\frac{d}{dx}\left(a_{ln}\frac{d\phi_n}{dx}\right)+\left(b_{ln}-b_{nl}\right)\frac{dh}{dx}\frac{d\phi_n}{dx}+c_{ln}\phi_n=0 \text{ for } l=-1, 0, 1, 2, \ldots, \tag{12}$$

with

$$a_{ln}=\left\langle f_l \middle| f_n \right\rangle, \tag{13}$$

$$b_{ln}=\left\langle f_l \middle| \frac{df_n}{dh} \right\rangle, \tag{14}$$

$$c_{ln}=c_{ln}^{(1)}\left(\frac{dh}{dx}\right)^2+b_{ln}\frac{d^2h}{dx^2}+c_{ln}^{(2)}, \tag{15}$$

$$c_{ln}^{(1)}=\left\langle f_l \middle| \frac{d^2 f_n}{dh^2} \right\rangle+\left(f_l\frac{df_n}{dh}\right)\Big|_{y=-h(x)}, \tag{16}$$

and

$$c_{ln}^{(2)}=\left\langle f_l \middle| \frac{\partial^2 f_n}{\partial y^2} \right\rangle+\left(f_l\frac{\partial f_n}{\partial y}\right)\Big|_{y=-h(x)}, \tag{17}$$

where the operator $\langle\cdot|\cdot\rangle$ is defined by

$$\left\langle F(y)\middle|G(y)\right\rangle=\int_{-h(x)}^{0}F(y)G(y)dy. \tag{18}$$

In Eqs. (12)-(17), the wavenumbers are also functions of $h(x)$; thus, the chain rule should be applied when performing differentiation with respect to h. For example,

$$\frac{df_n}{dh}=\frac{\partial f_n}{\partial h}+\frac{\partial f_n}{\partial k_n}\frac{dk_n}{dh} \tag{19}$$

where $\dfrac{dk_n}{dh}$ can be found from dispersion relation (9).

To introduce the boundary conditions of the CCMS, we use Eq. (6) to obtain

$$\Phi_-(x,y)=-\frac{\mathbf{i}g}{\omega}\frac{\cosh k_-\left(y+h_-\right)}{\cosh k_- h_-}\left(e^{\mathbf{i}k_- x}+Re^{-\mathbf{i}k_- x}\right)+\sum_{n=1}^{\infty}R_n f_n\left(y,h_-\right)e^{-\mathbf{i}k_n x} \tag{20}$$

and

$$\Phi_+(x,y)=-\frac{\mathbf{i}g}{\omega}\frac{\cosh k_+\left(y+h_+\right)}{\cosh k_+ h_+}\left(Te^{\mathbf{i}k_+ x}\right)+\sum_{n=1}^{\infty}T_n f_n\left(y,h_+\right)e^{\mathbf{i}k_n x} \tag{21}$$

for $x\le L_-$ and $x\ge L_+$, respectively. In Eqs. (20) and(21), R_n and T_n are unknown coefficients to be solved. For the matching condition at $x=L_-$, we can apply the conservations of mass and momentum, respectively, as

$$\left\langle f_l(y)\left|\frac{\partial\Phi_-(x,y)}{\partial x}\right|_{x=L_-}\right\rangle = \sum_{n=-1}^{\infty} b_{ln}\phi_n(L_-)\left.\frac{dh}{dx}\right|_{x=L_-}$$

for $l=-1, 0, 1, 2, \ldots$ (22)

and

$$\left\langle f_l(y)\middle|\Phi_-(L_-,y)\right\rangle = \sum_{n=-1}^{\infty} a_{ln}\phi_n(L_-) \text{ for } l=-1, 0, 1, 2, \ldots . \quad (23)$$

Eliminating R and R_n in Eqs. (20), (22) and (23) and using the definition (13) can result in

$$\sum_{n=-1}^{\infty}\left(\frac{d\phi_n}{d\mathbf{n}}(0+)a_{ln}+\phi_n(0+)\frac{dh}{d\mathbf{n}}(0+)b_{ln}-\mathbf{i}k_l\phi_n(0+)a_{\ln}\right)=-2\mathbf{i}k_0\delta_{l0}a_{00}$$

for $l=0, 1, 2, ..$ (24)

and

$$\sum_{n=-1}^{\infty}\left(\frac{d\phi_n}{d\mathbf{n}}(0+)a_{-1,n}+\phi_n(0+)\frac{dh}{d\mathbf{n}}(0+)b_{-1,n}\right)-\sum_{n=0}^{\infty}\mathbf{i}k_n\phi_n(0+)a_{-1,n}=-2\mathbf{i}k_0a_{-1,0} \quad (25)$$

with **n** the unit outward normal vector. We can obtain similar matching conditions at $x = L_+$ by dropping the right-hand side of Eqs. (24) and (25). Boundary conditions (24) and (25) were introduced by Porter and Staziker (1995) for the case in which the slopping-bottom mode is discarded.

Until now, no approximations have been involved. When numerical solutions are considered, the upper limits of both l and n should be truncated to N. Then, standard numerical methods, such as the finite difference or finite-element method (FEM), can be utilized to discretize Eq. (12). In this study, we use the generic finite-element library (Renard and Pommier, 2002) for numerical solutions. If M is the spatial degree of freedom for the FEM, we will roughly have an $M(N + 2)$ by $M(N + 2)$ sparse matrix, which is then solved by the SuperLU (James et al., 1999). If the MSS is considered, we can simply discard the sloping-bottom mode of the present formulation.

IV. EIGENFUNCTION MATCHING METHOD

Next, we will introduce the direct EMM solution for solving the water wave scattering problem defined in Section 2. According to most step methods, the bottom profile should be approximated by a succession of flat shelves, as depicted in Fig. 2.

In the figure, there are M shelves with depth h_m in intervals of $x_{m-1} < x < x_m$ for $m = 1, 2, 3, ..., M$ and $M-1$ steps at $x = x_m$ for $m = 1, 2, 3, ..., M-1$. To simplify the formulation, it is assumed that $x_0 = -\infty$ and $x_M = \infty$.

To apply the EMM, bottom boundary condition (5) is approximated by

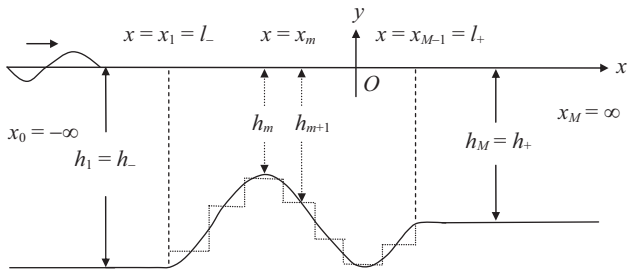

Fig. 2. Configuration of the EMM.

$$\frac{\partial\Phi_m}{\partial y}=0 \text{ on } y=-h_m \text{ for } x_{m-1}<x<x_m \text{ and } m=1, 2, ..., M \quad (26)$$

and

$$\frac{\partial\Phi}{\partial x}=0 \text{ on } x=x_m \text{ for } -h_m^{\max}<y<-h_m^{\min} \text{ and } m=1, 2, ..., M-1 \quad (27)$$

with $h_m^{\max} = \max(h_{m-1}, h_m)$ and $h_m^{\min} = \min(h_{m-1}, h_m)$. In Eq. (26), Φ_m is the solution on the mth shelf. In Eq. (27), the wall boundary condition is considered only for a deeper shelf. To match the solutions on shelves, the following matching conditions are required at each step:

$$\Phi_{m-1} = \Phi_m \quad (28)$$

and

$$\frac{\partial\Phi_{m-1}}{\partial x} = \frac{\partial\Phi_m}{\partial x} \quad (29)$$

on $x = x_m$ for $-h_m^{\min} < y < 0$ and $m = 1, 2, ..., M-1$.

According to the linear wave theory, a complete solution on the mth shelf can be constructed as

$$\Phi_m(x,y)=\sum_{n=0}^{\infty}\left(A_{m,n}e^{\mathbf{i}k_{m,n}(x-\bar{x}_{m-1})}+B_{m,n}e^{-\mathbf{i}k_{m,n}(x-\bar{x}_m)}\right)f_{m,n}(y) \text{ for } m=1, 2, ..., M \quad (30)$$

with $A_{m,n}$ and $B_{m,n}$ the unknown coefficients and

$$\begin{cases}\bar{x}_m = x_m \text{ for } m=1,2,...,M-1\\ \bar{x}_0=\bar{x}_M=0.\end{cases} \quad (31)$$

Furthermore, the eigenfunction, $f_{m,n}(y)$, is defined similarly to Eq. (8) as

$$f_{m,n}(y)=\frac{\cosh k_{m,n}(y+h_m)}{\cosh k_{m,n}h_m} \text{ for } n=0, 1, 2, ... \quad (32)$$

with wavenumber $k_{m,n}$ defined as

$$k_{m,n}\tanh k_{m,n}h_m = K \text{ for } m = 1, 2, ..., M \text{ and } n = 0, 1, 2, ... \tag{33}$$

Then, far field conditions (6) indicate that

$$\begin{cases} A_{1,0} = -\dfrac{\mathbf{i}g}{\omega} \\ A_{1,n} = 0 \text{ for } n = 1, 2, ..., N \\ B_{M,n} = 0 \text{ for } n = 0, 1, ..., N \end{cases} \tag{34}$$

and

$$\begin{cases} R = \dfrac{B_{1,0}}{A_{1,0}} \\ T = \dfrac{A_{M,0}}{A_{1,0}}. \end{cases} \tag{35}$$

Finally, the EMM can be constructed by considering the conservations of mass and momentum, respectively, as

$$\sum_{n=0}^{\infty}\mathbf{i}k_{m,n}\left(A_{m,n}e^{\mathbf{i}k_{m,n}\left(x_m-\bar{x}_{m-1}\right)} - B_{m,n}e^{-\mathbf{i}k_{m,n}\left(x_m-\bar{x}_m\right)}\right)\left\langle f_{m,n}\middle| f_{m,l}^{\max}\right\rangle$$
$$= \sum_{n=0}^{\infty}\mathbf{i}k_{m+1,n}\left(A_{m+1,n}e^{\mathbf{i}k_{m+1,n}\left(x_m-\bar{x}_m\right)} - B_{m+1,n}e^{-\mathbf{i}k_{m+1,n}\left(x_m-\bar{x}_{m+1}\right)}\right)\left\langle f_{m+1,n}\middle| f_{m,l}^{\max}\right\rangle \tag{36}$$

and

$$\sum_{n=0}^{\infty}\left(A_{m,n}e^{\mathbf{i}k_{m,n}\left(x_m-\bar{x}_{m-1}\right)} + B_{m,n}e^{-\mathbf{i}k_{m,n}\left(x_m-\bar{x}_m\right)}\right)\left\langle f_{m,l}^{\min}\middle| f_{m,n}\right\rangle$$
$$= \sum_{n=0}^{\infty}\left(A_{m+1,n}e^{\mathbf{i}k_{m+1,n}\left(x_m-\bar{x}_m\right)} + B_{m+1,n}e^{-\mathbf{i}k_{m+1,n}\left(x_m-\bar{x}_{m+1}\right)}\right)\left\langle f_{m,l}^{\min}\middle| f_{m+1,n}\right\rangle \tag{37}$$

for $m = 1, 2, ..., M-1$ and $l = 0, 1, ...,$ with

$$f_{m,l}^{\max}(y) = \begin{cases} f_{m+1,l}(y) & \text{if } h_{m+1} \ge h_m \\ f_{m,l}(y) & \text{if } h_m \ge h_{m+1} \end{cases} \tag{38}$$

$$f_{m,l}^{\min}(y) = \begin{cases} f_{m+1,l}(y) & \text{if } h_{m+1} \le h_m \\ f_{m,l}(y) & \text{if } h_m \le h_{m+1} \end{cases} \tag{39}$$

In Eqs. (36) and (37), the definition of $\langle\cdot|\cdot\rangle$ is extended from Eq. (18), with $h(x)$ replaced by the water depth corresponding to the first eigenfunction $F(y)$.

To perform numerical solutions, the upper limits of both l and n are truncated to N. Then, we have $(M-1)(N+1)$ linear equations from both Eqs. (36) and (37), and $2(N+1)$ linear equations from Eq. (34). These linear equations can be used for solving the $2M(N+1)$ unknowns $A_{m,n}$ and $B_{m,n}$. Then, the sought reflection and transmission coefficients can be found by using Eq. (35). Here, only connected shelves are related, as shown in Eqs. (36) and (37). As a result, the system matrix of the EMM is also highly sparse and will be solved by the sparse matrix solver SuperLU (James, et al., 1999).

V. NUMERICAL RESULTS

To obtain a firm error analysis for the CCMS, MSS, and EMM, numerical results are compared with Roseau's (1976) analytical solution and the semi-analytical solutions of IEM (Porter and Porter, 2000) for water wave scattering over sinusoidal shoal and slope. Here, the IEM solutions are obtained by a re-implementation from the first author. Specific reflection coefficients are tabulated for further reference and future studies. Furthermore, both the root-mean-square error (RMSE) and the maximum error (ME) are used in the following cases. M and N are the numbers of spatial degrees of freedom and evanescent modes, respectively, for all three models.

1. Roseau's bottom (Example I)

First, we consider Roseau's bottom, defined by

$$\beta x = \ln\mu + \frac{\varepsilon-1}{2}\ln\left(1+2\mu\cos\beta+\mu^2\right), \tag{40}$$

where

$$\mu = \left(\tan\frac{\beta\left(h(x)+1\right)}{1-\varepsilon}\right)\left(\sin\beta - \left(\tan\frac{\beta\left(h(x)+1\right)}{1-\varepsilon}\right)\cos\beta\right)^{-1}. \tag{41}$$

Eq. (40) defines a variable step of depths from 1 to ε; $\beta \in (0, \beta_{\max})$ is the steepness of the variable step with

$$\beta_{\max} = \pi - \tan^{-1}\frac{1-\varepsilon}{\sqrt{4\varepsilon}}. \tag{42}$$

Here, $\beta_{\max}$ is obtained by enforcing the positiveness condition of the bottom slope and is given explicitly for the first time, to the best of our knowledge. The analytical reflection coefficient was derived by Roseau (1976) as

$$|R| = \left|\frac{\sinh\pi\beta^{-1}\left(k_- - \varepsilon k_+\right)}{\sinh\pi\beta^{-1}\left(k_- + \varepsilon k_+\right)}\right|, \tag{43}$$

in which the wavenumbers k_- and k_+ are defined by

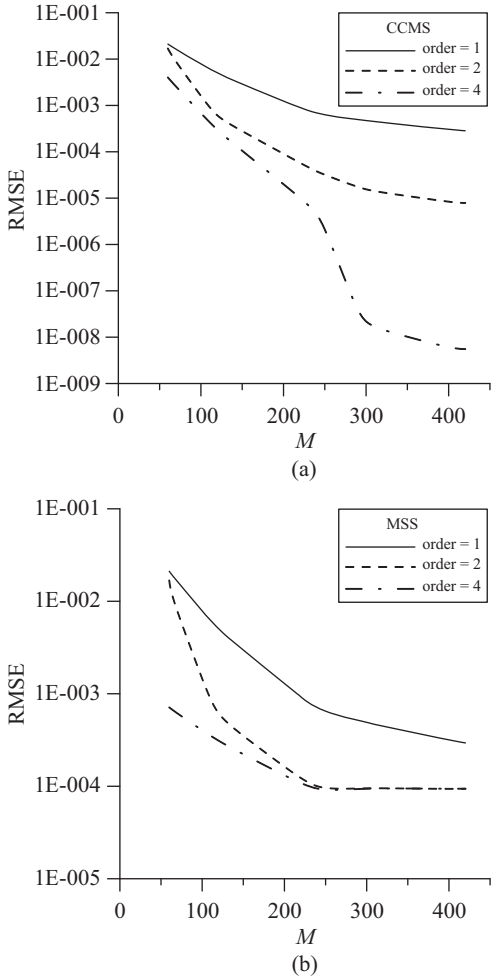

Fig. 3. RMSE comparison of different orders for (a) CCMS and (b) MSS.

$$K = k_- \tanh k_- = k_+ \tanh \varepsilon k_+ . \tag{44}$$

To perform an error analysis, we initially consider a case with $\varepsilon = 0.5$ and $\beta = 1.0$. The computational domain is established by $l_- \cong -17.5550$ and $l_+ \cong 8.77749$ such that

$$h(l_-) \cong 1 - 10^{-8} \tag{45}$$

and

$$h(l_+) \cong \varepsilon + 10^{-8}. \tag{46}$$

In addition, the RMSE and ME are evaluated between the numerical reflection coefficients and the analytical values obtained by Eq. (43) for $\omega^2/g = 0.5, 0.75, ..., 2.5$. The optimal error for the present configuration will be 10^{-8}, as suggested by Eqs. (45) and (46).

Before performing numerical solutions, we studied the order effect of FEM shape functions for the MSE-type models of CCMS and MSS. Fig. 3 shows that numerical solutions

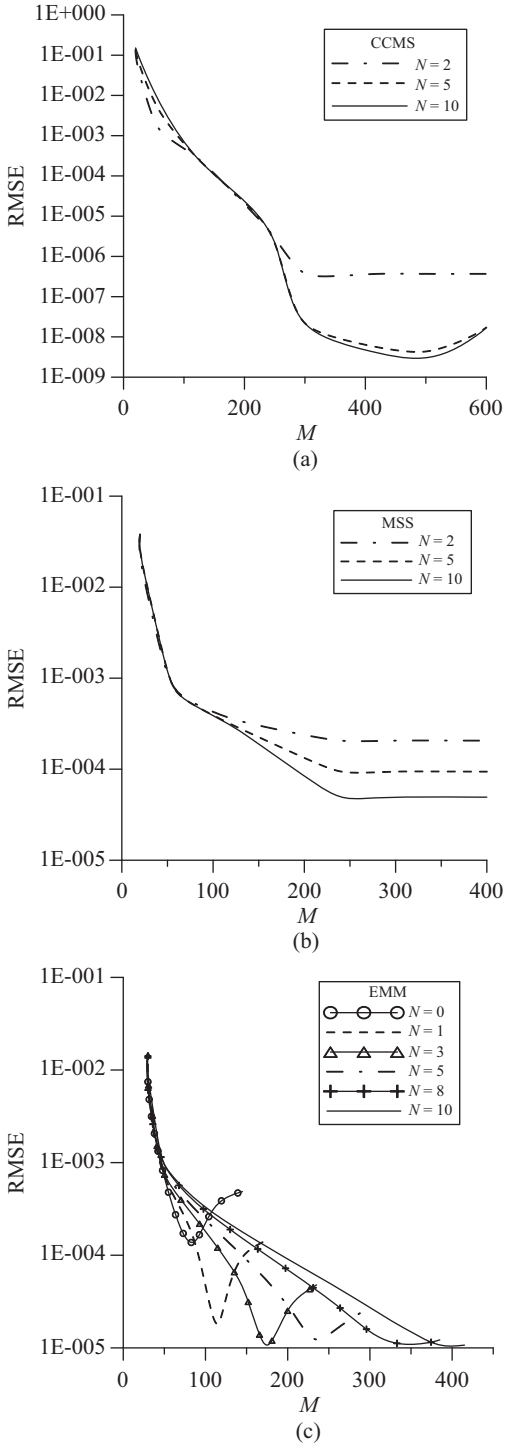

Fig. 4. RMSE comparison with different *M* and *N* of Roseau's case for (a) CCMS, (b) MSS, and (c) EMM.

obtained by higher-order shape functions significantly improve the accuracy, particularly when the sloping-bottom mode is included in the solution procedure. Therefore, we will adopt quartic elements for the MSE-type models in the following study.

Fig. 4 gives the numbers of spatial degrees of freedom versus RMSEs with different N for the numerical solutions

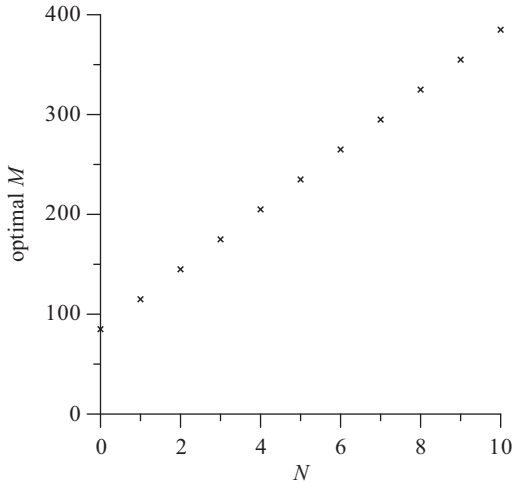

Fig. 5. Relation between the optimal *M* and *N* for the normal case of Roseau's bottom.

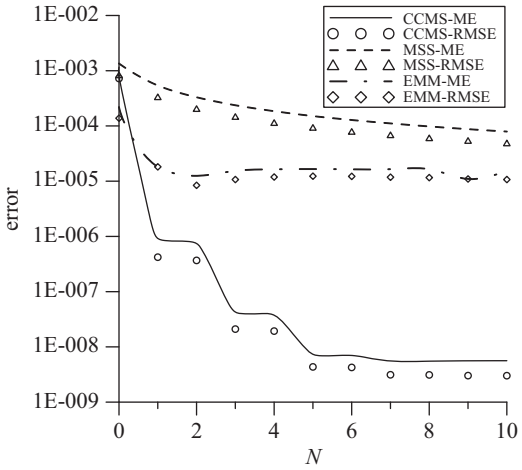

Fig. 6. Error comparisons with different *N* for the normal case of Roseau's bottom.

obtained by the CCMS, MSS, and EMM. These results suggest that the required M is essentially independent of N for the MSE-type models. Therefore, we selected $M = 500$ and $M = 300$, respectively, for the CCMS and MSS in this example. For the EMM solutions, we can observe that there is an optimal M value for every individual N, as shown in Fig. 4(c) and further explained in Fig. 5. In Fig. 5, a linear relation between N and the corresponding optimal M can be found.

Fig. 6 gives the numbers of evanescent modes versus the RMSEs and MEs for the three models. In the figure, the CCMS only requires $N = 5$ for obtaining numerical solutions with errors approaching the optimal value of 10^{-8}. Comparing the MSS and the EMM, the EMM requires much fewer evanescent modes ($N = 2$) for obtaining solutions with a similar accuracy of 10^{-5}, although optimal values of M should be used in the EMM, which is still a concern.

Table 1 addresses the computing times required for different configurations of the three models. Because all three models result in sparse system matrices, the numerical efficiencies are similar based on the total degrees of freedom. The EMM is slightly more efficient than the MSE-type models because it requires no numerical integrations.

Table 1. Computing times for the normal case of Roseau's bottom.

$kh = 0.5$ $\varepsilon = 0.5$ $\beta = 1$	Total degrees of freedom	Time (s)
CCMS ($M = 60$, $N = 0$)	120	0.15
CCMS ($M = 120$, $N = 0$)	240	0.25
CCMS ($M = 240$, $N = 0$)	480	0.46
CCMS ($M = 60$, $N = 2$)	240	0.57
CCMS ($M = 120$, $N = 2$)	480	0.99
CCMS ($M = 240$, $N = 2$)	960	1.88
CCMS ($M = 60$, $N = 5$)	420	0.87
CCMS ($M = 120$, $N = 5$)	840	3.35
CCMS ($M = 240$, $N = 5$)	1680	6.43
MSS ($M = 60$, $N = 0$)	60	0.07
MSS ($M = 120$, $N = 0$)	120	0.10
MSS ($M = 240$, $N = 0$)	240	0.18
MSS ($M = 60$, $N = 2$)	180	0.35
MSS ($M = 120$, $N = 2$)	360	0.61
MSS ($M = 240$, $N = 2$)	720	1.12
MSS ($M = 60$, $N = 5$)	360	1.26
MSS ($M = 120$, $N = 5$)	720	2.37
MSS ($M = 240$, $N = 5$)	1440	4.51
EMM ($M = 60$, $N = 0$)	60	0.01
EMM ($M = 120$, $N = 0$)	120	0.02
EMM ($M = 240$, $N = 0$)	240	0.46
EMM ($M = 60$, $N = 2$)	180	0.03
EMM ($M = 120$, $N = 2$)	360	0.08
EMM ($M = 240$, $N = 2$)	720	0.25
EMM ($M = 60$, $N = 5$)	360	0.09
EMM ($M = 120$, $N = 5$)	720	0.26
EMM ($M = 240$, $N = 5$)	1440	0.94

2. Roseau's Bottom (Example II)

To demonstrate the superiority of the EMM, with which multiple waves can be approximated by fewer shelves, we consider an extreme case with $\varepsilon = 0.1$, $\beta = \beta_{\max} - 10^{-3}$, and the computational domain is given by $l_- \cong -7.94328$ and $l_+ \cong 0.794322$ according to Eqs. (45) and (46). Both the CCMS and MSS fail in this example, due to the requirement of high spatial resolution for approximating the multiple waves and the extreme geometry with very large curvature and slope. For the EMM solution, Table 2 gives the numerical errors for different values of M with $N = 5$, in which the errors are evaluated by considering $\omega^2/g = 4, 4.25, \ldots, 6$, and the shelves are of equal lengths.

If we further examine the EMM solutions, we can find that a high resolution is required only for the rapidly varying part

Table 2. Accuracy comparison for the extreme case of Roseau's bottom.

$N = 5$	ME	RMSE
$M = 50$	1.31E-02	7.60E-03
$M = 100$	3.40E-02	3.29E-02
$M = 200$	1.05E-02	9.88E-03
$M = 300$	2.65E-03	2.36E-03
$\bar{M} = 2$	6.10E-03	5.04E-03
$\bar{M} = 4$	5.58E-03	4.75E-03
$\bar{M} = 6$	4.44E-03	3.98E-03
$\bar{M} = 8$	3.18E-03	3.18E-03
$\bar{M} = 10$	2.72E-03	2.30E-03

of the bottom profile. Therefore, we divide the computational domain into two regions separated at $x = l_0 \cong 0.0612120$, which is defined by

$$h(l_0) \cong 0.5. \tag{47}$$

In the rapidly varying region, we approximate the bottom profile by 29 uniform shelves, whose length is approximately equivalent to that of the previous configuration with $M = 300$. Table 2 gives the numerical errors for different shelf numbers, $\bar{M}$, in the left region. In the table, only $\bar{M} = 10$ shelves are required to obtain a numerical solution with similar accuracy to the previous configuration at $M = 300$. This demonstrated the superiority of the EMM over the MSE-type models.

3. Water Wave Scattering over a Sinusoidal Slope

Next, we consider the problem of water wave scattering over a sinusoidal slope defined by

$$h(x) = 0.55 - 0.45\sin\left(\frac{s}{0.45}x - \frac{\pi}{2}\right) \tag{48}$$

with $l_- = 0$, $l_+ = 0.45\pi/s$, $h_- = 1$, $h_+ = 0.1$, and s being a slope parameter. Two cases of short ($kh_+ = \pi$) and long ($kh_+ = \pi/10$) waves are considered.

For the short-wave case, Fig. 7 gives the numbers of spatial degrees of freedom versus RMSEs with different N for the numerical solutions obtained by the CCMS, MSS, and EMM. In the figure, the errors are evaluated compared to the IEM solution with $s = 2.7, 2.75, ..., 3.2$. In this case, we carefully re-implemented the IEM solution such that the accuracy is at least six decimal places, as addressed in Table 3 for $s = 3$. In the table, the notations of parameters can be referred to the literature of Porter and Porter (2000). Based on the results in Fig. 7, we typically consider $M = 36$ and $M = 16$ for the CCMS and the MSSs, respectively, in the short-wave case. For the EMM solutions, we select the optimal M value for every individual N, as further explained in Fig. 8, which shows a linear relation between N and its corresponding optimal M.

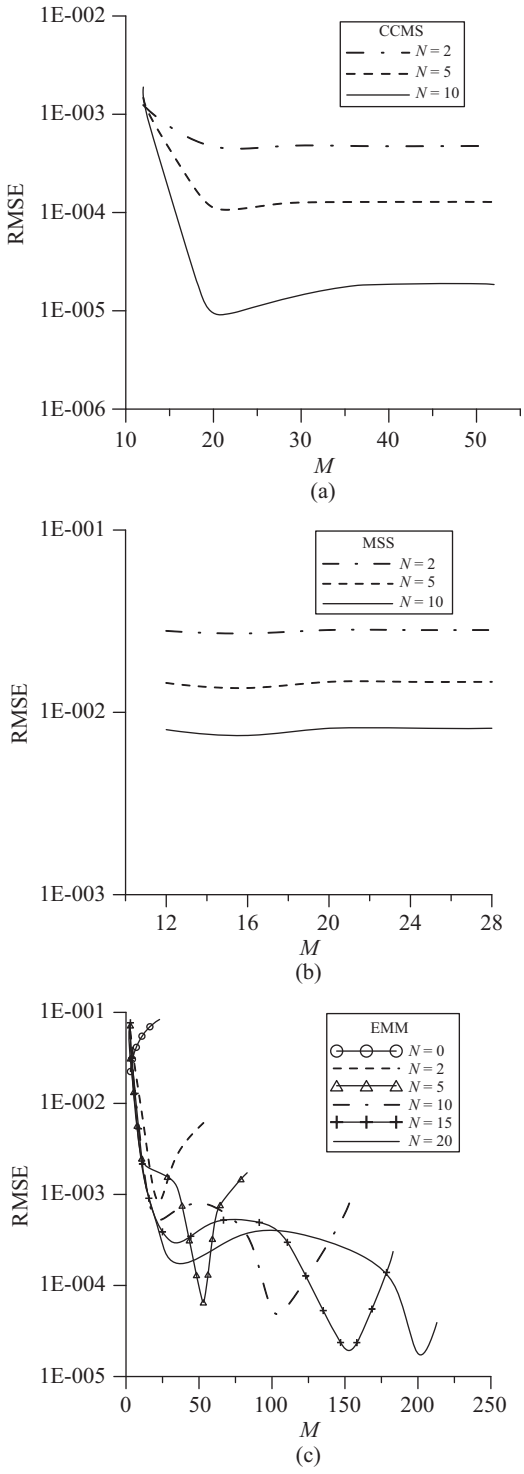

Fig. 7. RMSE comparison with different M and N of the short-wave sinusoidal slope for (a) CCMS, (b) MSS, and (c) EMM.

Fig. 9 gives errors versus N for all three models. In the figure, the CCMS requires $N = 25$ for obtaining numerical solutions with errors approaching the optimal value of 10^{-6}. At the same time, the computational efficiency of the CCMS is much higher than that of the IEM semi-analytical solution,

Table 3. IEM solutions for the short-wave sinusoidal slope.

N_1	N_2	$\tilde{Q}_{11}$	$\tilde{Q}_{12}$	$\tilde{Q}_{22}$	$\|R\|$	$\|T\|$	Time (s)
0	0	1.346206	3.085958	6.484078	0.133683	1.024239	85
2	2	0.987939	2.471228	5.337687	0.150134	1.021801	670
5	5	0.978752	2.434815	5.178499	0.148372	1.022076	2440
10	10	0.978421	2.434807	5.178429	0.148112	1.022116	7864
20	20	0.978375	2.434758	5.178397	0.148111	1.022117	25013
.	.	.	.	.	.	.	.
.	.	.	.	.	.	.	.
.	.	.	.	.	.	.	.
26	26	0.978372	2.434754	5.178371	0.148112	1.022117	43885
27	27	0.978372	2.434753	5.178370	0.148112	1.022117	47176
28	28	0.978372	2.434753	5.178370	0.148112	1.022117	50463

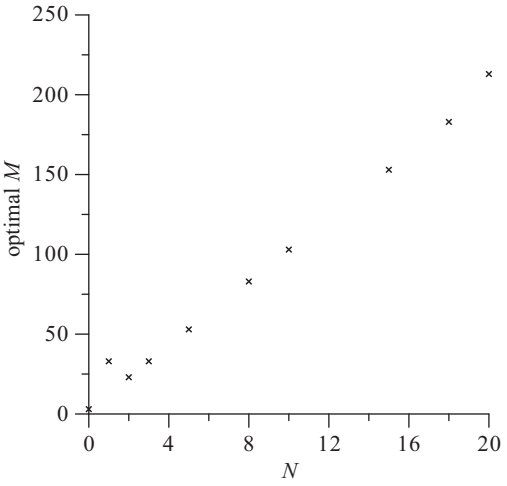

Fig. 8. Relation between optimal *M* and *N* for the short-wave sinusoidal slope.

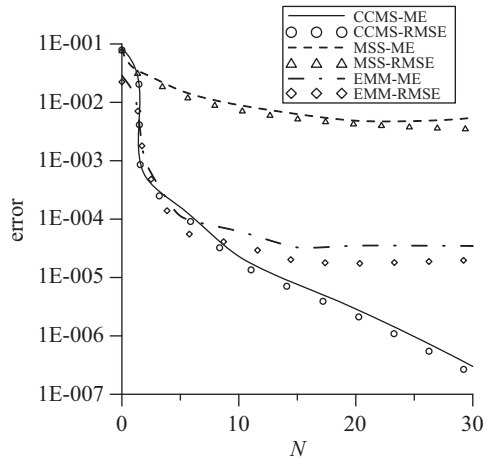

Fig. 9. Error comparison with different *N* for the short-wave sinusoidal slope.

which can be concluded from the typical computing times in Tables 1 and 3. In addition, the present case requires more evanescent modes than the first example of Roseau's bottom,

Table 4. Reflection coefficients obtained by CCMS (*N* = 25), MSS (*N* = 25), and EMM (*N* = 20) for the short-wave sinusoidal slope.

s	IEM/CCMS	MSS	EMM	MSS error	EMM-error
2.7	0.139122	0.142385	0.139087	3.26E-03	3.51E-05
2.75	0.140742	0.144078	0.140713	3.34E-03	2.89E-05
2.8	0.142310	0.137649	0.142287	4.66E-03	2.30E-05
2.85	0.143830	0.147308	0.143812	3.48E-03	1.76E-05
2.9	0.145302	0.148850	0.145289	3.55E-03	1.26E-05
2.95	0.146729	0.150346	0.146721	3.62E-03	7.90E-06
3	0.148111^{+}	0.151796	0.148108	3.68E-03	3.55E-06
3.05	0.149452^{+}	0.153204	0.149453	3.75E-03	4.50E-07
3.1	0.150753	0.145906	0.150757	4.85E-03	4.15E-06
3.15	0.152015	0.155898	0.152023	3.88E-03	7.58E-06
3.2	0.153240	0.157188	0.153251	3.95E-03	1.08E-05

which is expected due to the less smoothness of the present bottom at $x = l_-$ and $x = l_+$. On the other hand, the EMM only requires $N = 5$ for obtaining numerical solutions with accuracy better than 10^{-4} while including more evanescent modes provides negligible improvement.

Furthermore, the numerical results of both the CCMS and the EMM are more accurate than those of the MSS, as shown in Fig. 9. The detailed reflection coefficients are tabulated in Table 4, which can be adopted for comparison in further studies.

Here, the numerical values of the CCMS and IEM are essentially the same up to six decimal places; therefore, a unified column is provided for the two models. Furthermore, if the sixth decimal places of the two models are different by 1 due to round-off errors, a symbol $^{+}$ is added.

Additionally, we consider the long-wave case in which the errors are evaluated for s = 1.5, 1.55, ..., 2. Figs. 10 and 11 show the resulted RMSEs versus M and N, respectively. Based on Figs. 10(a) and (b), we selected $M = 36$ and $M = 12$, respectively, for the CCMS and the MSS in the long-wave case. The results are similar to those of the short-wave case, except slightly more evanescent modes are needed for the

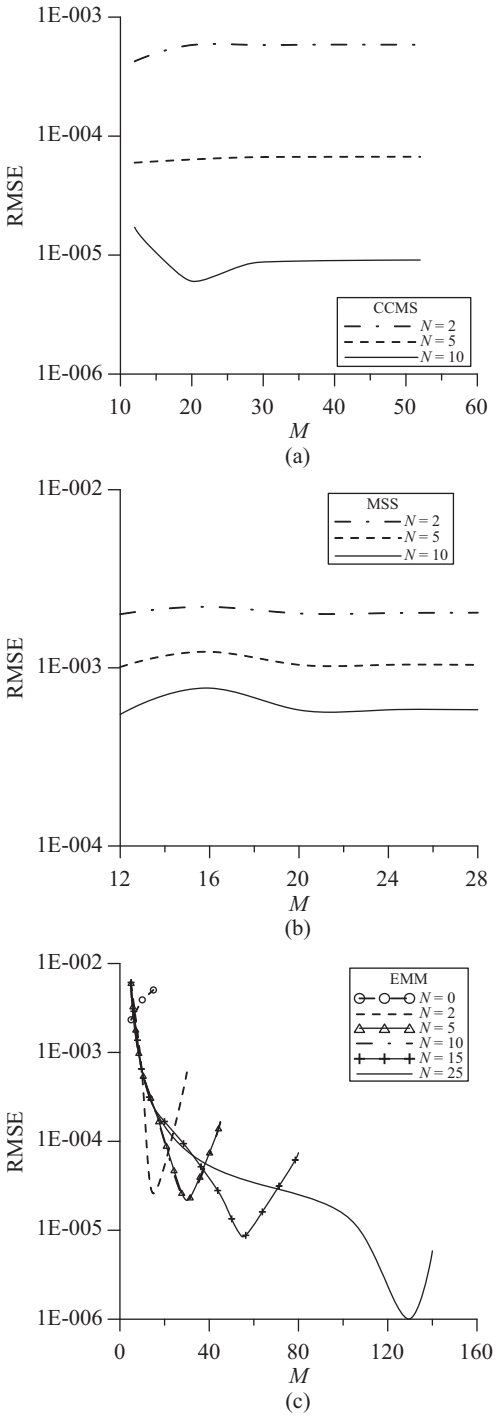

Fig. 10. RMSE comparison with different *M* and *N* of the long-wave sinusoidal slope for (a) CCMS, (b) MSS, and (c) EMM.

EMM and the accuracy of MSS improves slightly with N. Additionally, we provide the detailed reflection coefficients in Table 5 for comparison in future studies.

4. Water Wave Scattering over a Sinusoidal Shoal

Finally, we consider the problem of a water wave scattering over a sinusoidal shoal, defined by

Table 5. Reflection coefficients obtained by the CCMS (*N* = 25), MSS (*N* = 25), and EMM (*N* = 20) for the long-wave sinusoidal slope

s	IEM/CCMS	MSS	EMM	MSS error	EMM error
1.5	0.498580	0.498794	0.498582	2.14E-04	2.36E-06
1.55	0.499169	0.499383	0.499171	2.14E-04	2.32E-06
1.6	0.499707^{+}	0.499922	0.499710	2.15E-04	2.25E-06
1.65	0.500202	0.500416	0.500204	2.15E-04	2.18E-06
1.7	0.500657	0.500871	0.500659	2.15E-04	2.09E-06
1.75	0.501076^{+}	0.501291	0.501078	2.15E-04	2.00E-06
1.8	0.501465	0.501680	0.501467	2.15E-04	1.91E-06
1.85	0.501825	0.502040	0.501827	2.15E-04	1.83E-06
1.9	0.502160	0.502375	0.502162	2.15E-04	1.73E-06
1.95	0.502472	0.502688	0.502474	2.15E-04	1.65E-06
2	0.502764	0.502979	0.502765	2.15E-04	1.56E-06

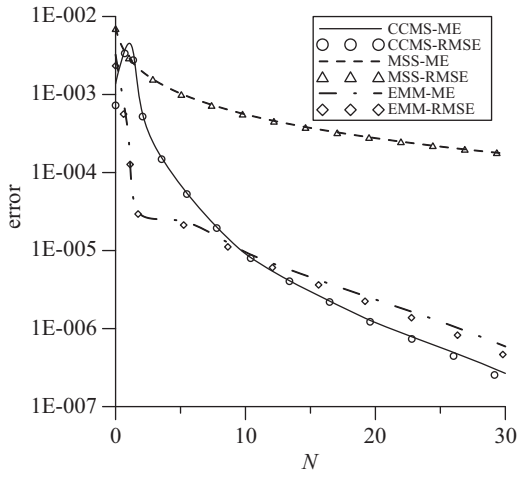

Fig. 11. Error comparison with different *N* for the long-wave sinusoidal slope.

$$h(x) = 0.55 - 0.45\sin\left(\frac{2\pi}{w}x - \frac{\pi}{2}\right) \tag{49}$$

with $l_{-} = 0$, $l_{+} = w$, $h_{-} = 1$, and $h_{+} = 0.1$, and w being a width parameter. Only a short-wave case ($kh_{+} = \pi$) is considered in this example. The errors are evaluated based on $w = 0.5$, 0.55, ..., 1.

Figs. 12 and 13 show the resulted RMSEs versus *M* and *N*, respectively. Based on Figs. 12(a) and (b), we selected *M* = 100 and *M* = 40, respectively, for the CCMS and MSSs in this example. Additionally, the optimal values of *M* are utilized for the EMM in Fig. 13. Compared with the sinusoidal-slope cases, larger numbers of *M* are required to obtain a similar level of accuracy. In Fig. 13, the CCMS and EMM are accurate up to six and four decimal places, respectively. Furthermore, their accuracy significantly improves over the

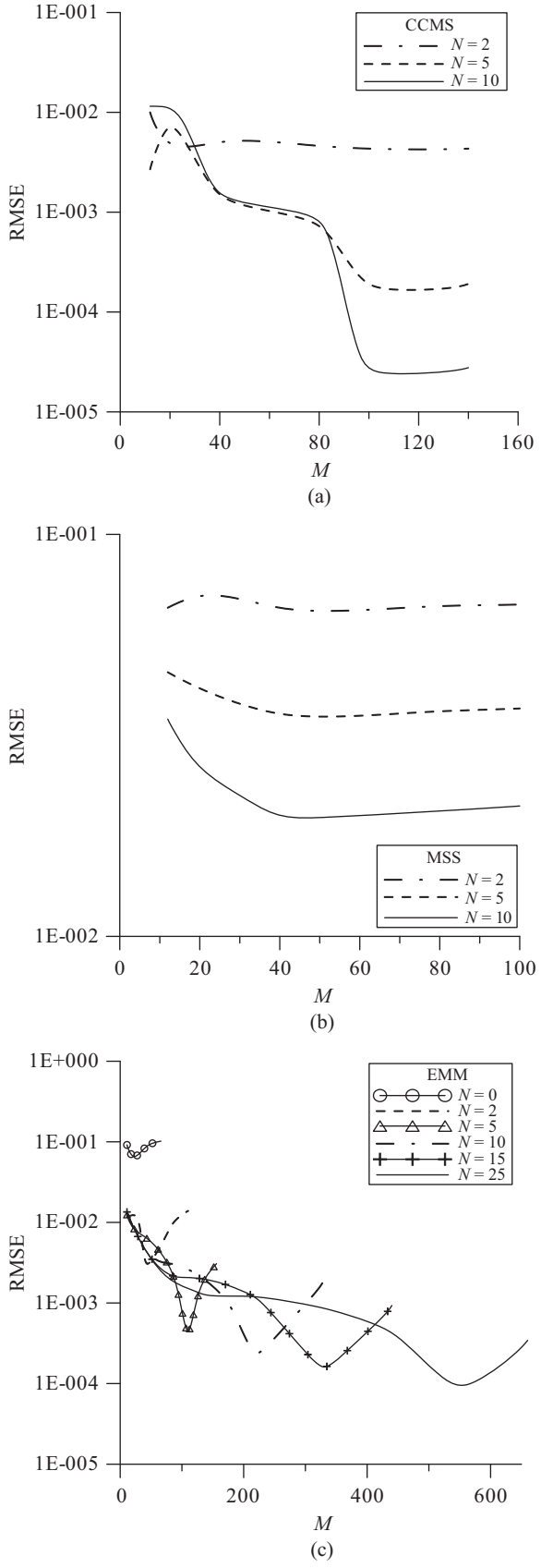

Fig. 12. RMSE comparison with different *M* and *N* of the sinusoidal shoal for (a) CCMS, (b) MSS, and (c) EMM.

Table 6. Reflection coefficients obtained by the CCMS (*N* = 40), MSS (*N* = 40), and EMM (*N* = 30) for the sinusoidal shoal.

w	IEM/CCMS	MSS	EMM	MSS error	EMM error
0.5	0.353932^{+}	0.361688	0.353979	7.76E-03	4.73E-05
0.55	0.345327^{+}	0.352615	0.345391	7.29E-03	6.35E-05
0.6	0.336311^{+}	0.339943	0.336380	3.63E-03	6.87E-05
0.65	0.326921^{+}	0.333387	0.326985	6.47E-03	6.42E-05
0.7	0.317194^{+}	0.320426	0.317245	3.23E-03	5.08E-05
0.75	0.307174^{+}	0.310330	0.307204	3.16E-03	2.93E-05
0.8	0.296907^{+}	0.302311	0.296907	5.40E-03	5.30E-07
0.85	0.286440^{+}	0.291516	0.286405	5.08E-03	3.48E-05
0.9	0.275823^{+}	0.279023	0.275747	3.20E-03	7.61E-05
0.95	0.265109	0.268368	0.264987	3.26E-03	1.22E-04
1.0	0.254348^{+}	0.257671	0.254175	3.32E-03	1.73E-04

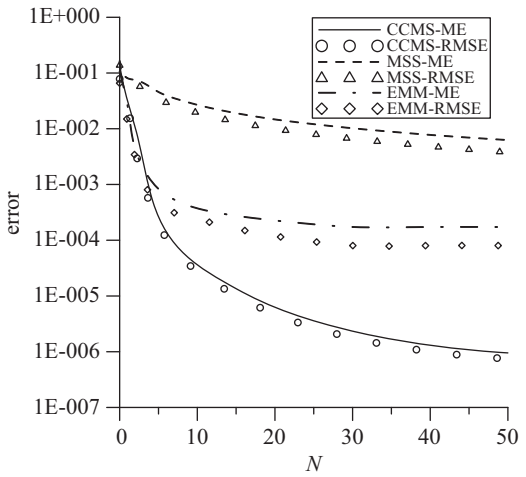

Fig. 13. Error comparison with different *N* for the sinusoidal shoal.

MSS. Finally, Table 6 addresses the detailed reflection coefficients for comparison in further studies.

VI. DISCUSSIONS AND CONCLUSION

Both the CCMS and the EMM are reviewed. To perform numerical studies, a generic FEM code is implemented for solving the MSE-type models of CCMS and MSS. Furthermore, quartic elements are adopted in the FEM numerical solution procedures. Sparse matrices are resulted for all of the CCMS, MSS, and EMM, which can be solved efficiently by a sparse matrix solver. These numerical results are compared with Roseau's analytical solution and the IEM semi-analytical solutions of sinusoidal bottoms, which are obtained from a re-implementation by the first author. Specific reflection coefficients are tabulated for comparison in future studies. The numerical solutions of the CCMS are accurate up to extreme values for all cases. The numerical solutions obtained by the EMM are accurate up to at least four decimal places. In

addition, their improvements in accuracy over the MSS are significant. For an extreme case of Roseau's bottom, only the EMM can produce reasonable solutions with few shelves.

Overall, the CCMS is in a relatively more mature stage of development than the EMM, which is currently limited to stationary problems in two-dimensional or three-dimensional axisymmetric domains. The application of the EMM beyond this limit is currently under investigation.

REFERENCES

Airy, G. B. (1845). On tides and waves. Encyclopedia Metropolitan, 241-396.

Athanassoulis, G. A. and K. A. Belibassakis (1999). A consistent coupled-mode theory for the propagation of small-amplitude water waves over variable bathymetry regions. J. Fluid Mech. 389, 275-301.

Athanassoulis, M. and K. Belibassakis (2009). A novel coupled-mode theory with application to hydroelastic analysis of thick, non-uniform floating bodies over general bathymetry. Proceedings of the Institution of Mechanical Engineers, Part M: Journal of Engineering for the Maritime Environment 223, 419-438.

Belibassakis, K. A. (2007). A coupled-mode model for the scattering of water waves by shearing currents in variable bathymetry. J. Fluid Mech. 578, 413-434.

Belibassakis, K. A., G. A. Athanassoulis and T. P. Gerostathis (2001). A coupled-mode model for the refraction-diffraction of linear waves over steep three-dimensional bathymetry. Applied Ocean Research 23, 319-336.

Belibassakis, K. and G. Athanassoulis (2002). Extension of second-order stokes theory to variable bathymetry. J. Fluid Mech. 464, 35-80.

Bender, C. J. and R. G. Dean (2003). Wave transformation by two-dimensional bathymetric anomalies with sloped transitions. Coast Eng. 50, 61-84.

Bender, C. J. and R. G. Dean (2005). Wave transformation by axisymmetric three-dimensional bathymetric anomalies with gradual transitions in depth. Coast Eng. 52, 331-351.

Berkhoff, J. C. W. (1972). Computation of combined refraction-diffraction. 13th International Conference on Coastal Engineering, Vancouver , 471-490

Chamberlain, P. G. and D. Porter (1995). The modified mild-slope equation. J. Fluid Mech. 291, 393-407.

Devillard, P., F. Dunlop and B. Souillard (1988). Localization of gravity waves on a channel with a random bottom. J. Fluid Mech. 186, 521-538.

James, W. D., C. E. Stanley, R. G. John, S. L. Xiaoye and W. H. L. Joseph (1999). A supernodal approach to sparse partial pivoting. SIAM J. Matrix Anal. Appl. 20, 720-755.

Kirby, J. T. (1986). A general wave equation for waves over rippled beds. J. Fluid Mech. 162, 171-186.

Kirby, J. T. and R. A. Dalrymple (1983). Propagation of obliquely incident water waves over a trench. J. Fluid Mech. 133, 47-63.

Massel, S. R. (1993). Extended refraction-diffraction equation for surface waves. Coast Eng. 19, 97-126.

Mei, C. C. and J. L. Black (1969). Scattering of surface waves by rectangular obstacles in waters of finite depth. J Fluid Mech 38, 499-511.

Miles, J. W. (1967). Surface-wave scattering matrix for a shelf. J. Fluid Mech. 28, 755-767.

Newman, J. N. (1965). Propagation of water waves over an infinite step. J. Fluid Mech. 23, 399-415.

O'Hare, T. J. and A. G. Davies (1992). A new model for surface wave propagation over undulating topography. Coast Eng. 18, 251-266.

O'Hare, T. J. and A. G. Davies (1993). A comparison of two models for surface-wave propagation over rapidly varying topography. Applied Ocean Research 15, 1-11.

Porter, D. and D. J. Staziker (1995). Extensions of the mild-slope equation. J. Fluid Mech. 300, 367-382.

Porter, R. and D. Porter (2000). Water wave scattering by a step of arbitrary profile. J. Fluid Mech. 411, 131-164.

Renard, Y. and J. Pommier (2002). Getfem++. An open source generic c++ library for finite element methods. Technical report, http://home.gna.org/getfem

Rey, V. (1992). Propagation and local behaviour of normally incident gravity waves over varying topography. European journal of mechanics B, Fluids 11, 213-232.

Rey, V. (1995). A note on the scattering of obliquely incident surface gravity waves by cylindrical obstacles in waters of finite depth. European journal of mechanics B, Fluids 14, 207-216.

Roseau, M. (1976). Asymptotic wave theory. North-Holland Pub. Co., Amsterdam: New York

Seo, S.-N. (2014). Transfer matrix of linear water wave scattering over a stepwise bottom. Coast Eng. 88, 33-42.

Takano, K. (1960). Effets d'un obstacle parallelepipedique sur la propagation de la houle. La Houille Blanche 15, 247-267.

Tsai, C. C., T.-W. Hsu and Y.-T. Lin (2011). On step approximation for roseau's analytical solution of water waves. Mathematical Problems in Engineering 2011.

Tsai, C. C., Y.-T. Lin and T.-W. Hsu (2013). On the weak viscous effect of the reflection and transmission over an arbitrary topography. Phys. Fluids 25, 043103-043121.

Tsai, C.-C., Y.-T. Lin and T.-W. Hsu (2014). On step approximation of water-wave scattering over steep or undulated slope. International Journal of Offshore and Polar Engineering 24, 98-105.